Solid State Ionics 270 (2015) 54–60

Contents lists available at ScienceDirect

Solid State Ionics

journal homepage: www.elsevier.com/locate/ssi

High temperature crystal chemistry of the n = 3 Ruddlesden–Popper phase $LaSr_3Fe_{1.5}Co_{1.5}O_{10-\delta}$

F. Prado [a,*], A. Abate [a,b], J.V. Castillo [a], A. Caneiro [b], G. Cuello [c]

[a] Departamento de Física, Universidad Nacional del Sur e Instituto de Física del Sur, CONICET, Av. L.N. Alem 1253, 8000 Bahía Blanca, Argentina
[b] Instituto Balseiro and Centro Atómico Bariloche, CNEA, Av. Bustillo 9500, 8400 S. C. de Bariloche, Argentina
[c] Institut Laue-Langevin, BP 156, F-38042 Grenoble Cedex 9, France

ARTICLE INFO

Article history:
Received 6 August 2014
Received in revised form 4 December 2014
Accepted 9 December 2014
Available online 23 December 2014

Keywords:
$LaSr_3Co_{1.5}Fe_{1.5}O_{10-\delta}$
Ruddlesden–Popper phases
Neutron Powder Diffraction
Mixed conductors
SOFC cathodes

ABSTRACT

The crystal chemistry of the n = 3 Ruddlesden–Popper phase $LaSr_3Co_{1.5}Fe_{1.5}O_{10-\delta}$ has been studied in the temperature range $20 \le T \le 900$ °C by in situ Neutron Powder Diffraction (NPD), and thermogravimetric and linear expansion measurements. The presence of oxygen vacancies at the O(2) and O(4) crystal sites, in the central perovskite layer, along with the variation of the bottleneck space available for oxygen migration with temperature at T > 300 °C indicates the O(4)–O(4) jumps predominate during oxide ion diffusion. Absolute oxygen content measurements support oxygen excess (>10.0) at temperatures below 300 °C, which is unusual for the n = 3 R–P phases. The total expansion in the temperature range $25 \le T \le 900$ °C, $\alpha = \frac{\alpha_V}{3} = 26.5\ (1) \times 10^{-6}\ K^{-1}$, is twice the values reported for the electrolytes. The linear expansion along the c-axis, $\alpha_c = 34.15\ (1) \times 10^{-6}\ K^{-1}$, is mainly absorbed by the perovskite block while the width of the rock salt layers remains nearly constant. Additionally, the oxygen chemical expansivity (β_C) value determined for this layered compound, $\beta_C = 0.670$, was found to be approximately three times larger than those reported for the three dimensional perovskite system $La_{1-x}Sr_xCoO_{3-\delta}$.

1. Introduction

The search for new oxides exhibiting mixed oxide-ion and electronic conductivity for electrochemical applications such as oxygen separation membranes and cathodes for intermediate solid oxide fuel cells (IT-SOFC) has stimulated the study of the high temperature properties of the Ruddlesden–Popper series of oxides $A_{n+1}B_nO_{3n+1}$ with A = La, Sr and B = Fe,Co,Ni and *n* = 1, 2 and 3 [1–4]. The crystal structure of these materials consists of *n* perovskite layers alternating with rock salt layers stacked along the *c* axis as shown in Fig. 1 for n = 3. As the number of perovskite layers increases from n = 1 to ∞, the R–P phases gradually lose the two-dimensional feature of the n = 1 phases, reaching the three dimensional limit for the perovskite (n = ∞) [5]. In the case of the R–P series $(La,Sr)_{n+1}(Fe,Co)_nO_{3n+1}$, both the electrical and the oxide ion conductivities increase as the number *n* of perovskite layers and the Co content increases [3,6]. Armstrong et al. [7] have reported that the limit of Co solubility for the n = 3 R–P solid solution $LaSr_3Fe_{3-x}Co_xO_{10-\delta}$ is x = 1.5. In addition, the authors have found that the crystal structure of this compound remains stable with no structural transformations occurring up until 900 °C even under an argon atmosphere [7]. Thus, the electrochemical behavior of $LaSr_3Fe_{1.5}Co_{1.5}O_{10-\delta}$ at high temperature is attractive to study. Moreover, Lee and Manthiram [8] have reported that the power density obtained from a SOFC prepared with $LaSr_3Fe_{1.5}Co_{1.5}O_{10-\delta}$ as cathode electrode is comparable to the one obtained using the perovskite $La_{0.6}Sr_{0.4}CoO_{3-\delta}$.

The electrochemical performance of $LaSr_3Fe_{1.5}Co_{1.5}O_{10-\delta}$ as cathode electrode and most of its relevant properties at high temperature such as the electronic and oxide ion conductivities, oxygen reduction reaction, and chemical expansivity are affected by the oxygen defect structure. Therefore, knowledge of it helps understand the mechanisms taking place at the cathode during the oxygen reduction reaction. Previous studies have shown that $LaSr_3Fe_{1.5}Co_{1.5}O_{10-\delta}$ exhibits large oxygen nonstoichiometry with values of δ varying from 0 to 1 as the temperature increases and the oxygen partial pressure decreases [7]. The oxygen atoms are located at four different crystallographic sites, the O(1) and O(4) crystal sites located in the $(Fe,Co)O_2$ layers, the O(3) in the rock salt layer and the O(2) site connecting the octahedra along the *c* axis (see Fig. 1). Previous studies on NPD data at both room temperatures [9] and in situ at high temperature [10], have been carried out on the n = 3 R–P phases $(La,Sr)_4(Fe,Al)_3O_{10-\delta}$, with majority of Fe in the B site. The analysis of the data have located the oxygen vacancies at the O(2) and O(4) crystal sites. In particular for $La_{0.9}Sr_{3.1}Fe_3O_{10-\delta}$, Kagomiya et al. [10] have reported that the majority oxygen vacancy concentration changes from O(2) to O(4) as the temperature increases.

* Corresponding author. Tel.: +54 291 4595168, +54 291 4595101x2830.
E-mail address: fernando.prado@uns.edu.ar (F. Prado).

http://dx.doi.org/10.1016/j.ssi.2014.12.007
0167-2738/

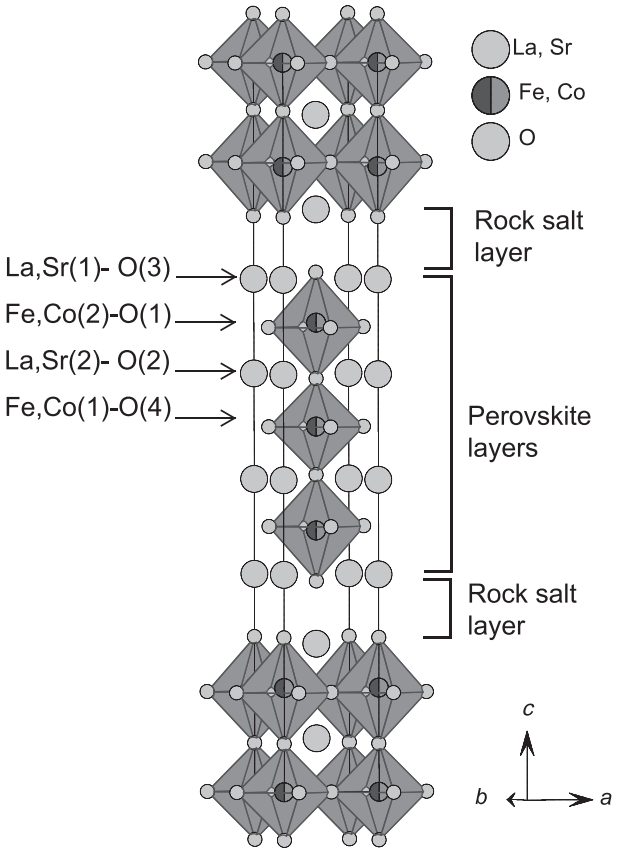

Fig. 1. Crystal structure of the n = 3 Ruddlesden–Popper phase $LaSr_3Fe_{1.5}Co_{1.5}O_{10-\delta}$.

Aiming to study the effects of the substitution of Fe by Co on the crystal chemistry, and therefore on the factors controlling the oxide ion diffusion mechanism of the n = 3 R–P phase $LaSr_3Fe_{1.5}Co_{1.5}O_{10-\delta}$ at high temperatures, we have carried out in situ high temperature NPD data, thermogravimetric and linear expansion measurements. Based on these data we determined the oxygen defects in the temperature range $20 < T < 900$ °C and the effects of the thermal and chemical contributions on the volume expansion, and on the oxide ion diffusion mechanism for this layered compound.

2. Experimental

The $LaSr_3Fe_{1.5}Co_{1.5}O_{10-\delta}$ (LSCFO) sample was synthesized by solid-state reaction. Stoichiometric amounts of La_2O_3, previously dried overnight at 1000 °C in air, $SrCO_3$, Fe_2O_3, and Co_3O_4 were mixed and ground with a mortar and pestle and heat treated at 1000 °C for 12 h in air. Subsequently, the powder was ball milled during 15 min using an agate milling media and heat treated at 1325 °C for 18 h. Then, the sample was cooled down at room temperature at a rate of 1 °C/min under pure oxygen, with intermediate dwells at 700, 500, 400 and 300 °C during 10 h to maximize the oxygen content of the phase. Additionally, a fraction of the sample was annealed at 800 °C under pure oxygen at 200 atm and cooled down at room temperature at a rate of 1 °C/min with intermediate dwells at 800, 700, 600 and 500 °C during 8 h at each temperature.

The formation of the LSFCO phase was verified by X-ray diffraction (XRD) at room temperature with a Philips PW1700 diffractometer using Cu Kα radiation and a graphite monochromator. The reflections were indexed according to the tetragonal unit cell (space group *I4/mmm*). A small percentage (<2%) precipitates in a perovskite phase (La,Sr)(Fe,Co)O_3. The final product was stored in a sealed glass tube under vacuum at room temperature to prevent water adsorption.

The neutron diffraction experiments were carried out in Grenoble at the Institute Laue–Langevin on the D2B ($\lambda = 1.594$ Å and $10 \le 2\theta \le 150°$) powder diffractometer at T = 25, 250, 500, 700 and 900 °C in air. For measurements at room temperature the samples prepared under pure oxygen at 1 and 200 atm were placed in a vanadium sample holder, while for measurements at T ≥ 250 °C the sample was placed into a quartz tube with an open top, which allowed oxygen exchange with the surrounding air. Initially the NPD patterns were fitted using constant scale matching profile (LeBail Method) and afterwards the crystal structure was refined by the Rietveld method using the FullProf suite tools [11]. The profile of the diffraction peaks was fitted using a Pseudo-Voigt function. The background of the Neutron Powder Diffraction data obtained at 20 °C was refined with a polynomial function, while a linear interpolation of N selected points ($50 < N < 80$) was used at T ≥ 250 °C, when the quartz tube was used as a sample holder. The cell parameters, atomic positions, oxygen sites occupancies, and isotropic thermal parameters were modified during the refinement of the crystal structure. The total oxygen content used during the refinements were the values obtained from iodometric titration [12] on samples heat treated at 250, 500, 700 and 900 °C during 12 h, in air, and subsequently quenched at room temperature and on samples cooled down at room temperature under 1 atm and 200 atm of pure O_2.

The reduction of $LaSr_3Co_{1.5}Fe_{1.5}O_{10-\delta}$ was performed heating the sample up to 1040 °C in dry H_2, in a highly sensitive thermogravimetry equipment [13] consisting of a symmetrical thermobalance, based on a Cahn 1000 electrobalance. The thermobalance permits to detect mass changes within ± 10 μg, i.e. for a sample of about 0.5 g of $LaSr_3Co_{1.5}Fe_{1.5}O_{10-\delta}$, the resolution in the oxygen content is ± 0.001.

The linear expansion of $LaSr_3Co_{1.5}Fe_{1.5}O_{10-\delta}$ was measured on a cylindrical sample of approximately 5.0 mm diameter and 4 to 5 mm height, from room temperature to 900 °C, using a LINSEIS L75PT Series dilatometer. The sample was heated up to 900 °C at 5 °C/min, and, after a 1 h dwell, it was cooled at room temperature at a rate of 1 °C/min. The sample was then once again heated up to 900 °C at a rate of 1 °C/min, in air. The experimental data were corrected using Al_2O_3 as a standard.

3. Results and discussion

The crystal chemistry of $LaSr_3Fe_{1.5}Co_{1.5}O_{10-\delta}$ was determined from NPD data at room temperature on samples cooled under pure O_2 at pressures of 1 atm and 200 atm. Additionally, NPD data were recorded in situ at 250, 500, 700 and 900 °C, in air. In all the cases, the crystal structure was refined using the Rietveld method on the basis of the tetragonal space group *I4/mmm*. As an example Fig. 2a and 2b display the NPD data recorded at 20 °C for the sample cooled under 1 atm of O_2 and the data obtained in situ at 900 °C under air, respectively. The calculated profiles, their difference with the experimental data and the position of the allowed reflections of the tetragonal phase (S.G. *I4/mmm*) are also shown. During the refinements, the total oxygen content of the samples was fixed according to the values determined from iodometric titration, while the occupancies of the oxygen crystal sites were refined. No correlation was found between the thermal parameters and the oxygen occupancy for the sites O(1), O(2), O(3) and O(4). Fig. 3a shows the variation of the total oxygen content as a function of temperature, as determined from iodometric titration. Noteworthy, the total oxygen content of the sample cooled under 1 atm of O_2 is higher than 10.0. A similar result was obtained for the sample prepared under a pressure of 200 atm of O_2 whose value as determined from iodometry was 10.20 ± 0.01. Oxygen excess has been reported for the n = 1 R–P phases A_2BO_4 (A = La, Pr, Nd and B = Ni, Cu and Co) [14,15], and has been located in the tetrahedral sites defined by the Ln atoms in the rock salt layer. Furthermore, an interstitial mechanism for the oxide ion diffusion was indicated for La_2NiO_4 [16,17]. In the case of the $LaSr_3Fe_{1.5}Co_{1.5}O_{10-\delta}$ phase, the tetrahedral sites are located in the position Oi (8 g, 0, ½, z) of the *I4/mmm* space group. The refinement of the NPD data of the samples cooled under 1 atm and 200 atm

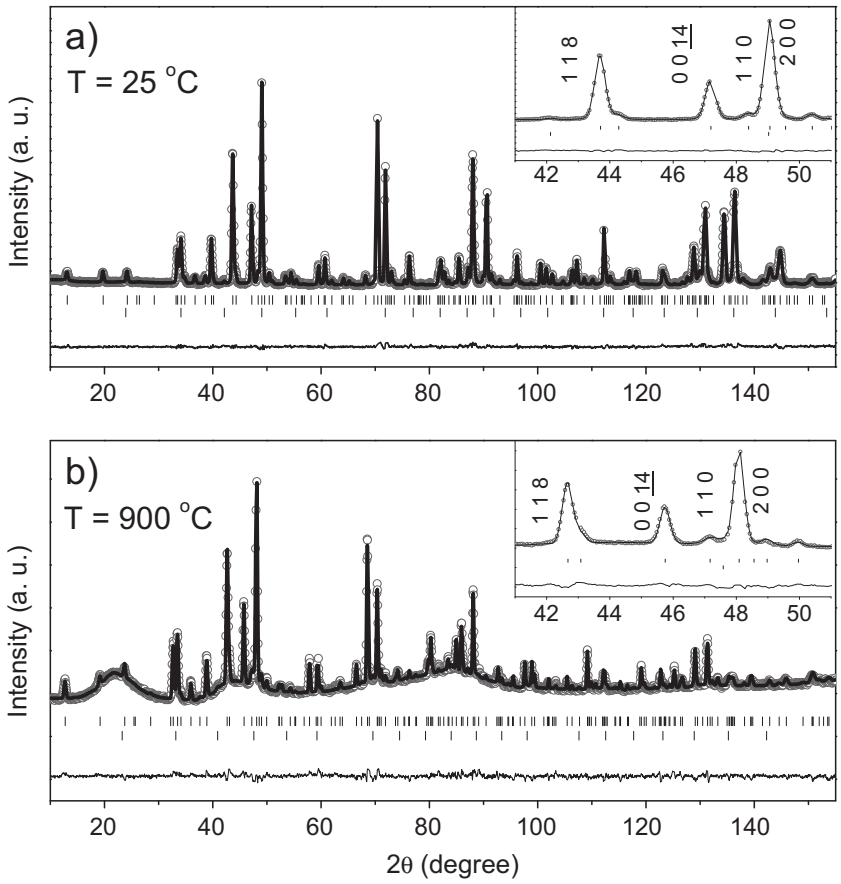

Fig. 2. Representative NPD data of $LaSr_3Fe_{1.5}Co_{1.5}O_{10-\delta}$ at 25 and 900 °C in air. The insets expand the 2θ range $42 \le 2\theta \le 50$ (degree) to appreciate in more detail the quality of the refinements.

of O_2, showed that all the oxygen crystal sites were fully occupied. Then, the oxygen excess was incorporated allowing oxygen ions at the crystal site Oi (8 g, 0, 1/2, z) with z = ¼. In this case, it was necessary to constrain the thermal factor B(Oi) = 1 Å^2. However, the quality of the refinements for these samples slightly improves, making it difficult to assess the presence of this kind of defects from our NPD data.

As the temperature increases, the oxygen content of the sample decreases due to the removal of oxygen atoms from the O(2) (4e, 0, 0, z) crystal site connecting the octahedra along the c-axis and the O(4) (4c, 0, ½, 0) crystal site at the central (Fe,Co)O_2 layer of the perovskite block. On the other hand, the O(1) (0, 1/2, z) and O(3) (0,0,z) crystal sites located at the perovskite block and the rock salt layer, respectively, were found to be always fully occupied. At T > 500 °C, the oxygen vacancy concentration at O(4) was larger than that at the O(2) crystal sites (see Fig. 3b), at T = 900 °C they reached ~17% and ~8%, respectively. In Table 1, we list the crystal structure parameters obtained from the refinement of the NPD data for $LaSr_3Co_{1.5}Fe_{1.5}O_{10-\delta}$ for the samples cooled down under pure O_2 at pressures of P = 1 and 200 atm at 20 °C and in situ at 900 °C.

In order to determine the total oxygen content at room temperature of the $LaSr_3Co_{1.5}Fe_{1.5}O_{10-\delta}$ sample originally prepared under P = 200 atm of O_2, we carried out thermogravimetric measurements according to the following sequence: a) a heating/cooling cycle was performed by steps in the temperature range $100 \le T \le 285$ °C in dry air while recording the mass variation and, b) the sample we reduced by heating up to 1040 °C at a heating rate of 4 °C/min in dry H_2. In both cases the variation of the mass of the sample with both time and temperature was recorded; these values were converted to oxygen content values after the reduction of the sample in dry H_2 was completed.

Fig. 4 shows the variation of the oxygen content as a function of time during the reduction of the sample as well as the heating profile. The oxygen content of the sample slightly varies up to T ~ 150 °C (point A). Then, the sample loses oxygen atoms continuously up to T ~ 440 °C where a plateau (point C) can be observed. Between points A and C there is a kink at ~330 °C (point B). As the temperature increases up to 1040 °C, the sample continues to lose oxygen atoms until the oxygen content gets to point D, which corresponds to a totally reduced sample formed by La_2O_3, SrO, and metallic Fe and Co as final products. Using point D as reference it was possible to calculate the variation of the oxygen content of the sample during the reduction. Thus, the plateau at the oxygen content $10-\delta = 8.25$ (point C) and the kink close to $10-\delta = 9.0$ (point B) correspond to the average oxidation states +2.5 and +3.0, respectively, for the transition metals. Finally, the oxygen content determined for the point A was $10-\delta = 10.043 \pm (1)$. Thus, the thermogravimetric run indicates the presence of oxygen excess at low temperature, in agreement with the oxygen content value obtained by iodometric titration for the sample prepared under 1 atm of O_2, and also with the analysis of NPD data, which insinuates, although not conclusively, the possibility of oxygen excess.

In Fig. 5 we show the behavior of the oxygen content in the low temperature range $100 \le T \le 300$ °C, in air, when the temperature is raised by steps (solid circles) from 100 °C to 220 (point A), 250 (point B) and 285 °C (point C). The inset in Fig. 5 shows the same data as a function of time. After the temperature is increased, the oxygen content of the sample decreases. For each temperature the oxygen content stabilizes at the values of 10.04 at point A, 10.025 at point B, and 10.007 at point C. After reaching point C, the sample was cooled to T = 220 °C (open squares). During cooling the oxygen content increases and reaches the

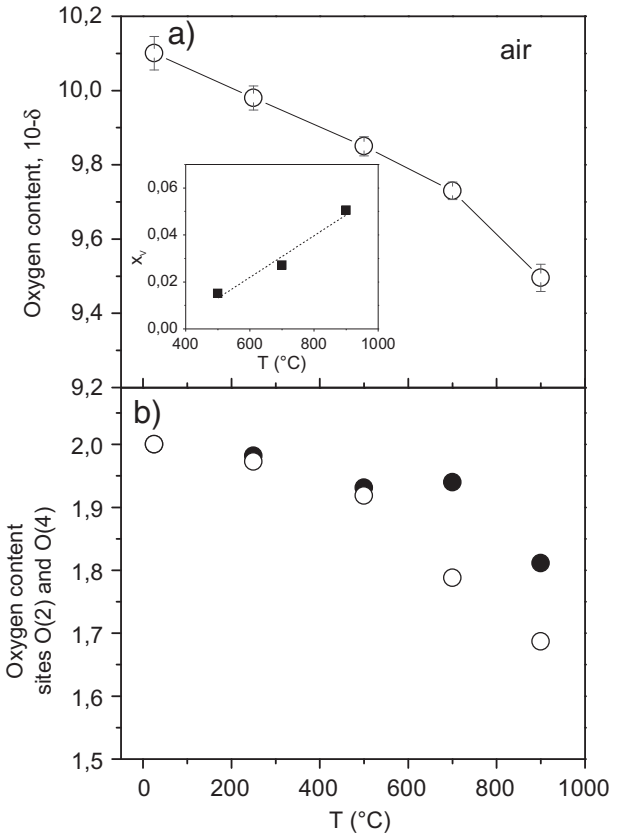

Fig. 3. a) Variation of the total oxygen content of $LaSr_3Fe_{1.5}Co_{1.5}O_{10-\delta}$ as a function of temperature determined by iodometric titration. The variation of the oxygen vacancies mole fraction, X_V, with temperature is shown in the inset, along with the linear fit used for calculations of the chemical expansivity β_C. b) Occupancy of the crystal sites O(2) and O(4) determined from "in situ" high temperature NPD measurements.

Table 1
Refined crystal structure parameters[a] from NPD data of $LaSr_3Fe_{1.5}Co_{1.5}O_{10-\delta}$ samples cooled down to 20 °C under: a) 1 atm of pure O_2, b) 200 atm of pure O_2, and c) in situ at 900 °C, in air.

			T = 20 °C pO_2 = 1 atm	T = 20 °C pO_2 = 200 atm	T = 900 °C
Atom	Site	$a = b$ (Å)	3.840 (2)	3.839 (2)	3.914 (1)
		c (Å)	27.875 (2)	27.87 (2)	28.723 (2)
La/Sr(1)	4e	z	0.568 (2)	0.568 (2)	0.573 (1)
		B_{iso} (Å^2)	0.48 (1)	0.53 (1)	2.46 (4)
La/Sr(2)	4e	z	0.701 (3)	0.701 (3)	0.702 (2)
		B_{iso} (Å^2)	0.28 (2)	0.29 (2)	1.90 (5)
Fe/Co(1)	2a	B_{iso} (Å^2)	0.35 (1)	0.26 (1)	1.65 (5)
Fe/Co(2)	4e	z	0.139 (2)	0.139 (2)	0.142 (2)
		B_{iso} (Å^2)	0.22 (1)	0.17 (1)	1.53 (3)
O(1)	8 g	z	0.138 (2)	0.138 (2)	0.137 (3)
		B_{iso} (Å^2)	0.50 (5)	0.55 (5)	2.4 (3)
O(2)	4e	z	0.069 (1)	0.07 (1)	0.065 (3)
		B_{iso} (Å^2)	0.87 (2)	0.79 (2)	4.70 (3)
		O_{cc}	1.00 (2)	1.00 (2)	0.906 (4)[b]
O(3)	4e	z	0.210 (2)	0.211 (2)	0.212 (4)
		B_{iso} (Å^2)	0.70 (1)	0.77 (1)	3.4 (4)
O(4)	4c	B_{iso} (Å^2)	0.92 (5)	0.67 (5)	4.25 (4)
		O_{cc}	1.00 (2)	1.00 (2)	0.842 (5)[b]
O_i	8 g	B_{iso} (Å^2)	1.0	1.0	–
		O_{cc}	0.025	0.05	–
		R_{wp}	8.98	11.5	14.5
		χ^2	1.9	2.1	2.5

[a] Space Group: I4/*mmm*; Atomic positions are (La/Sr)(1): (0,0,z); (La/Sr)(2): (0,0,z); (Fe/Co)(1): (0,0,0); (Fe/Co)(2): (0,0,z); O(1): (0,0.5,z); O(2): (0,0,z); O(3): (0,0,z); O(4): (0,0.5,0); and Oi:(0, 1/2,1/4).

[b] The occupancies of crystal sites O(2) and O(4) at 900 °C were constrained in such a way the sum of all the oxygen occupancies reproduce the total oxygen content determined by iodometry.

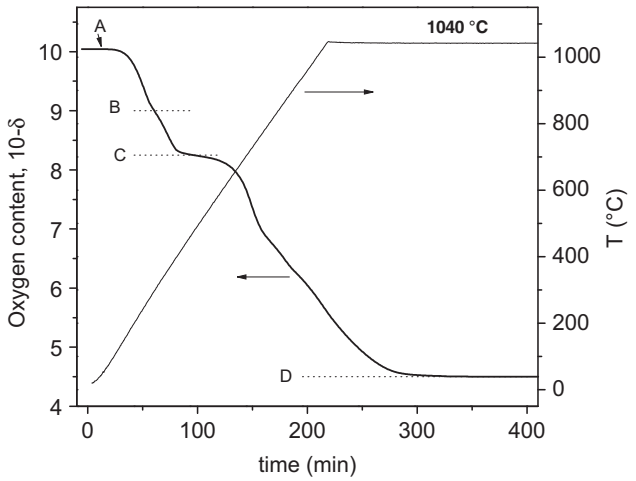

Fig. 4. Variation of the oxygen content as a function of time during the reduction of $LaSr_3Fe_{1.5}Co_{1.5}O_{10-\delta}$ in dry hydrogen. The temperature profile during the reduction is also shown.

value of point A, showing that the reduction/oxidation is reversible in the range of temperature where the oxygen content of the sample is >10.0. Subsequently the sample was cooled down to 100 °C and reduced in dry H_2 as described before.

The presence of oxygen excess in the rock salt layers of the n = 1 R–P phases causes the tilt of the octahedra MO_6 (M = Cu,Ni,Co) of the perovskite layer, inducing a crystal structure transformation from tetragonal to orthorhombic [14,15]. Although, our experimental data indicate the likelihood of oxygen excess at low temperature in $LaSr_3Co_{1.5}Fe_{1.5}O_{10}$, no evidence of a structural transformation was detected, suggesting the fraction of oxygen excess may be too low to cause a distortion of the octahedra arrangement and thereby a crystal structure transformation.

Fig. 6a shows the variations of the lattice parameters *a* and *c* of $LaSr_3Co_{1.5}Fe_{1.5}O_{10-\delta}$ with temperature. While the lattice parameter *a* changes almost linearly, the rate of change of lattice parameter *c* increases above T = 300 °C due to the removal of oxygen atoms from the crystal structure. This effect is also reflected by the variation of the relative change of the unit cell volume, $\Delta V/V_0$, as a function of temperature (Fig. 3b). For comparison, the $\Delta V/V_0$ vs. T curve obtained from linear expansion measurements is also included in Fig. 3b. The linear expansion was converted to volume expansion data through the relation $\frac{\Delta V}{V_0} \approx 3\frac{\Delta L}{L_0}$. The behavior of the relative volume expansion obtained from NPD and dilatometry show good agreement in the whole temperature range.

The total volume expansion in transition metal oxides depends mainly on temperature and oxygen nonstoichiometry, which are responsible for the thermal and chemical expansion contributions, respectively [18,19]. From simple thermodynamic relations, and neglecting variables other than temperature and oxygen nonstoichiometry [18,19], the variation of the linear expansion with temperature at constant pO_2 is described by

$$\left.\frac{\partial \varepsilon}{\partial T}\right)_{pO_2} = \frac{\beta_T}{3} + \frac{\beta_C}{3}\left.\frac{\partial x_v}{\partial T}\right)_{pO_2} \quad (1)$$

where $x_V = \frac{\delta}{10}$ is the oxygen vacancy molar fraction, $\varepsilon = \frac{\Delta L}{L_0}$, and $\beta_T = \frac{1}{V}\left.\frac{\partial V}{\partial T}\right)_{X_V}$ and $\beta_C = \frac{1}{V}\left.\frac{\partial V}{\partial x_V}\right)_T$ are the thermal and chemical expansivity, respectively. As the variation of the oxygen content in the low temperature range $20 \le T \le 300$ °C is small, ~ 0.4% according to thermogravimetric data (Fig. 5b), we can neglect $\left.\frac{\partial x_v}{\partial T}\right)_{pO_2}$ in Eq. (1), obtaining $\frac{1}{3}\beta_T = 15.46(1) \times 10^{-6}\ K^{-1}$ from the slope of the $\frac{\Delta V}{V_0}$ vs. *T* curve

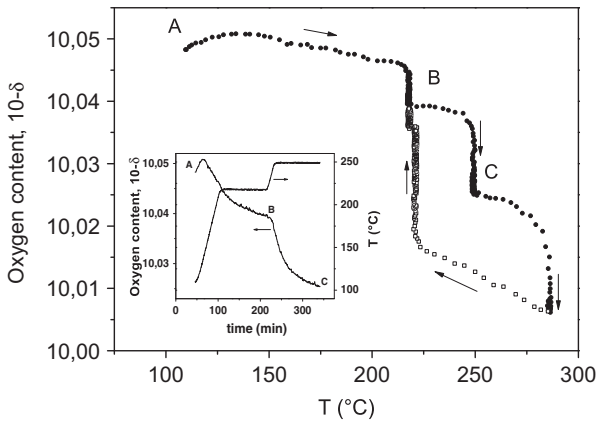

Fig. 5. Variation of the oxygen content of $LaSr_3Fe_{1.5}Co_{1.5}O_{10-\delta}$ with temperature in the temperature range $100 \le T \le 300$ °C in dry air. The inset shows the same experimental data as a function of time.

in Fig. 6b. In the same way, we can estimate β_C from Eq. (1) using the values $3 \times \frac{\partial \varepsilon}{\partial T}\Big)_{pO_2} = 1.060\ (2) \times 10^{-4}\ K^{-1}$ and $\frac{\partial x_v}{\partial T}\Big)_{pO_2} = 8.9\ (1.5) \times 10^{-5}\ K^{-1}$ determined by the linear fitting of the $\frac{\Delta V}{V_0}$ vs. T curve (Fig. 6b) and x_V vs T data (inset in Fig. 3a), respectively, in the temperature range $500 \le T \le 900$ °C. Thus, the value obtained for the oxygen vacancy chemical expansivity $\beta_C = 0.67\ (9)$ for $LaSr_3Co_{1.5}Fe_{1.5}O_{10-\delta}$ is approximately three times the values of β_C reported for the perovskites $La_{1-x}Sr_xCoO_{3-\delta}$, which is in the range $0.209 \le \beta_C \le 0.270$ when x_V varies between 0.015 and 0.05 [18]. Finally, the expansion coefficients were calculated from NPD data using the expression,

$$\alpha_p = \frac{1}{3}\frac{(p-p_0)}{p_0}\frac{1}{\Delta T}\Big|_{pO_2=cte}, \quad (2)$$

in the temperature range $25 \le T \le 900$ °C, in which p stands for the lattice parameters and the unit cell volume, and p_0 represents the parameter's values at the temperature of reference, $T_0 = 25$ °C. The obtained results are, $\alpha_a = 21.7\ (1) \times 10^{-6}\ K^{-1}$, $\alpha_c = 34.1\ (1) \times 10^{-6}\ K^{-1}$, and $\alpha = 1/3\ \alpha_v = 26.5\ (1) \times 10^{-6}\ K^{-1}$. The expansion along the c-axis is visibly larger than that observed along the a or b-axis and is related to the chemical expansion and the two dimensional feature of the crystal structure.

The chemical expansion of the crystal structure is a consequence of the removal of oxygen atoms from the O(2) and O(4) positions, these crystal sites behave like positive charge that cause the relaxation of the surrounding ions. Fig. 7 shows the variation with temperature of the distance between several ions and the cation (Fe,Co)(1), projected on the c-axis. While the cations (La,Sr) (2) and (Fe,Co) (2) move away, the O(2) oxygen ions move towards the oxygen vacancy on the c direction. As a consequence of these relative displacements, the (Fe,Co)(2) cation is located above the equatorial plane of the $(Fe,Co)O_6$ octahedra forming an angle O(2)–(Fe,Co)(1)–O(1) lesser than 90° (see the inset in Fig. 7b). Additionally, Fig. 8 shows how the linear expansion

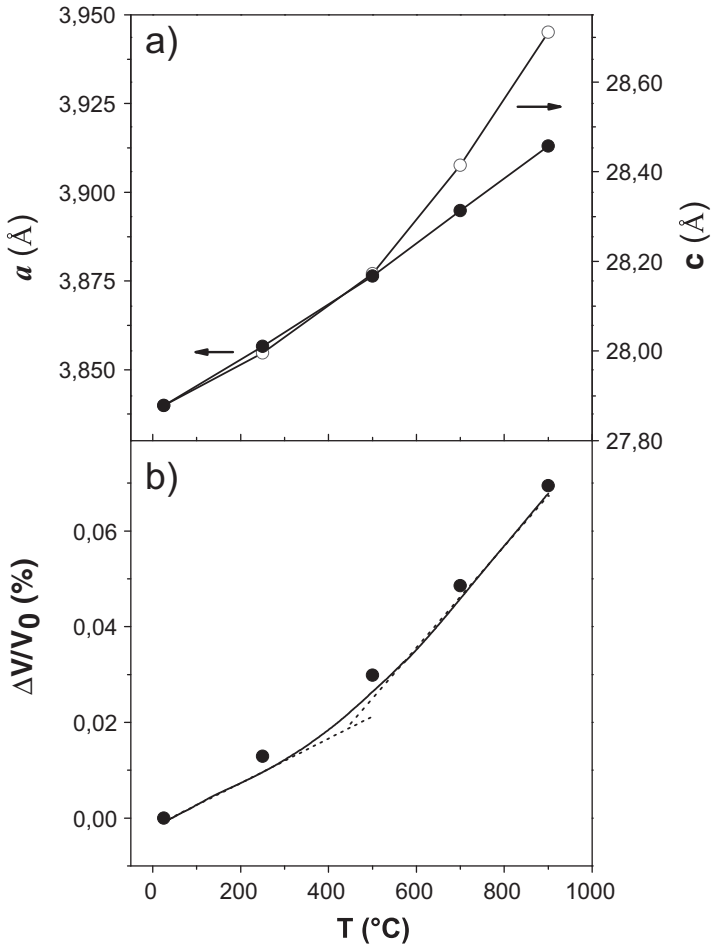

Fig. 6. Structural data of $LaSr_3Fe_{1.5}Co_{1.5}O_{10-\delta}$ as a function of temperature: a) Lattice parameters a and c and b) relative volume change determined from NPD data (solid circles) and dilatometry measurements (solid line). The straight lines correspond to the linear fit of the $\Delta V/V_0$ vs. T curve at the temperature ranges $20 \le T \le 300$ and $500 \le T \le 900$ °C.

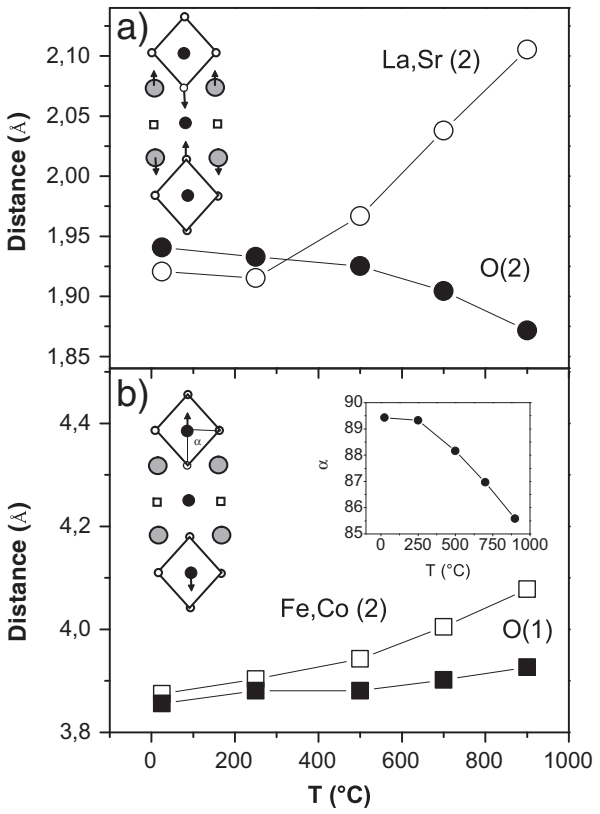

Fig. 7. Variation of the distances separating the cations (La,Sr) (1), (Fe,Co)(2), O(1) and O(2) with (Fe,Co)(1) projected along the c-axis.

observed along the c-axis is almost totally absorbed by the perovskite block (d_p), while the width of the rock salt layer (d_{rs}) remains practically constant in the whole temperature range, as was also observed in the case of the n = 2 R–P phases $Sr_3FeCoO_{6+\delta}$ and $Sr_3Fe_2O_{6+\delta}$ [20,21]. Finally, Fig. 9 shows the variation with temperature of the area of the triangles S_1 and S_2 defined by the cations (La,Sr)(2)–(La,Sr)(2)–(Fe,Co(1). These areas are a measure of the bottleneck space available for the oxide ions to migrate from the O(2) to the O(4) crystal site (area S_1) and from one O(4) to another (area S_2). These critical areas are one of the most relevant parameters to be considered for oxygen migration [22]. The inset in Fig. 9 shows the projection of these triangles on the y–z plane. Both triangles, S_1 and S_2, increase their sizes when the temperature varies from room temperature to 900 °C, however, while the area of S_2

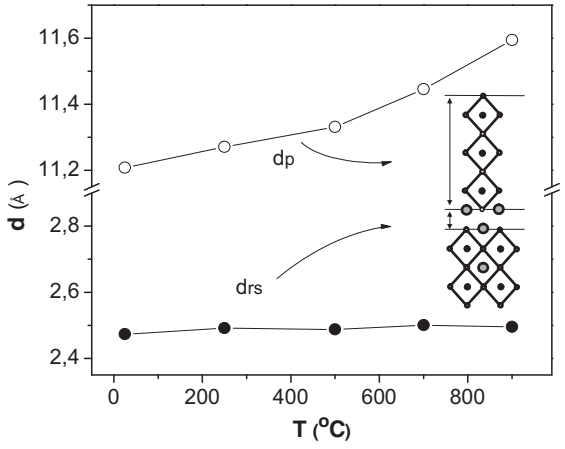

Fig. 8. Variation of the width of the perovskite and rocksalt blocks with temperature in $LaSr_3Fe_{1.5}Co_{1.5}O_{10-\delta}$.

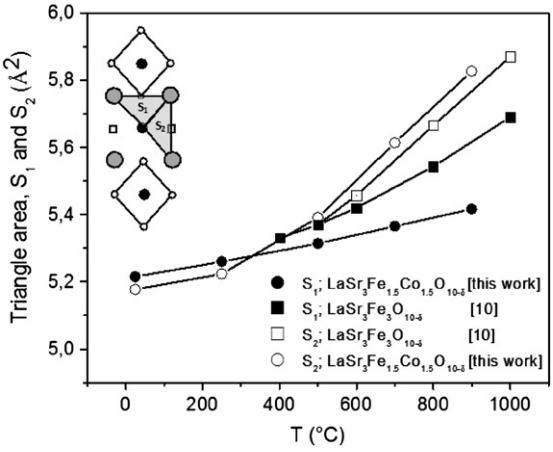

Fig. 9. Area of the triangles S_1 and S_2 defined by the cations (La,Sr)(2)–(La,Sr)(2)–(Fe, Co(1) as a function of temperature.

increases ~12.5%, S_1 expands only 4.6%. This is a consequence of the larger expansion observed along the c-axis (Fig. 6a) and the fact that the perovskite block mostly absorbs the thermal and chemical expansion along the c-axis (Fig. 8). For comparison, the S_1 and S_2 values determined from NPD data for $LaSr_3Fe_3O_{10-\delta}$ by Kagomiya et al. [10], are included in Fig. 9. The presence of Co in the perovskite block decreases the expansion of S_1 and increases that of S_2. This leads to a bigger difference between S_1 and S_2 at high temperature for the sample containing Co.

The crystal structure behavior described above becomes useful to discuss the oxide-ion diffusion mechanism in this mixed conductor at high temperature. For the cubic perovskites with mixed valence transition metals and large oxygen nonstoichiometry, the oxide-ion diffusion takes place via an oxygen vacancy mechanism [23]. Experimental evidence [20,21,24,25] also showed that oxide ion diffusion in the n = 2 R–P phases $Sr_3FeMO_{7-\delta}$ with M = Fe, Co and Ni occurs through a vacancy mechanism. In the case of the n = 3 R–P phase $LaSr_3Co_{1.5}Fe_{1.5}O_{10-\delta}$, the large oxygen vacancy concentration located at the O(2) and O(4) crystal sites indicates that a vacancy mechanism prevails for the oxide ion migration at high temperature using O(4)–O(4) and O(2)–O(4) jumps along the (Fe,Co)(1)O_6 octahedra edges. Moreover, since the expansion with temperature of the area S_2 is faster than that of S_1, the migration barrier for the O(4)–O(4) jumps should be lower than that corresponding to the O(2)–O(4) jumps suggesting the O(4)–O(4) jumps predominate for the oxide ion diffusion as was previously proposed by Kagomiya et al. [10] for the n = 3 R–P phase without cobalt, $LaSr_3Fe_3O_{10}$. The relative expansion of S_2 compared to S_1 increases with the incorporation of Co, likely increasing the predominance of the O(4)–O(4) jumps at high temperature. On the other hand, the presence of oxygen excess, as determined from thermogravimetric measurements, led us to speculate that an interstitial oxygen mechanism could play a role below ~300 °C, however more research is needed to validate this point.

4. Conclusions

The oxygen defect structure of the n = 3 R–P phase $LaSr_3Co_{1.5}Fe_{1.5}O_{10-\delta}$ has been determined in the temperature range $20 \leq T \leq 900$ °C by in situ Neutron Powder Diffraction (NPD), and thermogravimetric measurements. The analysis of NPD data obtained in situ at T > 300 °C, verified the presence of oxygen vacancies at the O(2) and O(4) crystal sites in the perovskite central layer, similar to $LaSr_3Fe_3O_{10-\delta}$, supporting a vacancy mechanism for oxide ion diffusion. The bottleneck space available for oxygen migration, S_1 and S_2, defined by the triangle areas enclosed by the cations (La,Sr)(2)–(La, Sr)(2)–(Fe,Co)(1), increases with temperature, however, S_2 increases

faster than S_1, suggesting that O(4)–O(4) jumps predominate during oxide ion diffusion. Our data indicates this predominance increases with the Co content. Thermogravimetric measurements as well as iodometry suggest the presence of oxygen excess (>10.0) at temperatures below 300 °C, which is unusual for n = 3 R–P phases. The chemical expansivity (β_C) of $LaSr_3Co_{1.5}Fe_{1.5}O_{10-\delta}$, in air, $\beta_C = 0.670$, indicates that oxygen exchange with the atmosphere in the layered compound $LaSr_3Co_{1.5}Fe_{1.5}O_{10-\delta}$ causes volume changes approximately three times larger than the values reported for $La_{1-x}Sr_xCoO_{3-\delta}$. As the temperature increases, the chemical expansion contribution causes a relative larger expansion along the c-axis in comparison to the expansion along the *a*-axis, which is mainly absorbed by the perovskite block as the width of the rock salt layer remains constant.

Acknowledgments

This work was supported by CNEA (Argentine Atomic Energy Commission), CONICET (Argentine Research Council) and ANPCyT, Argentina, through PICT 2010-0322 and PICT 2013-1032. We are also grateful to MINCYT, Argentina, for special financial support to collect NPD data at the ILL, Grenoble, France.

References

[1] V.V. Vashook, N.E. Trofimenko, H. Ullman, L.V. Makhnach, Solid State Ionics 131 (2000) 329–336.
[2] G. Amow, I.J. Davison, S.J. Skinner, Solid State Ionics 177 (2006) 1205–1210.
[3] A. Manthiram, F. Prado, T. Armstrong, Solid State Ionics 152 (2002) 647.
[4] S. Nishimoto Takahashi, M. Matsuda, M. Miyake, J. Am. Ceram. Soc. 93 (2010) 2329–2333.
[5] S.N. Ruddlesden, P. Popper, Acta Crystallogr. 11 (1958) 54–55.
[6] A. Manthiram, J.-H. Kim, Y.N. Kim, K.T. Lee, J. Electroceram. 27 (2011) 93–107.
[7] T. Armstrong, F. Prado, A. Manthiram, Solid State Ionics 140 (2001) 89–96.
[8] K.T. Lee, A. Manthiram, Chem. Mater. 18 (2006) 1621–1626.
[9] J.Y. Lee, J.S. Swinnea, H. Steinfink, W.M. Reiff, S. Pei, J.D. Jorgensen, J. Solid State Chem. 103 (1993) 1.
[10] I. Kagomiya, K. Jimbo, K. Kamimoto, J. Solid State Chem. 207 (2013) 184–189.
[11] J. Rodríguez-Carvajal, Fullprof: a program for Rietveld refinement and profile matching analysis of complex powder diffraction patterns, Laboratoire Léon Brillouin (CEA-CNRS), France, 2002.
[12] A. Manthiram, S. Swinnea, Z.T. Sui, H. Steinfik, J.B. Goodenough, J. Am. Chem. Soc. 109 (1987) 6667–6669.
[13] A. Caneiro, P. Bavdaz, J. Fouletier, J.P. Abriata, Sci. Instrum. 53 (1982) 1072.
[14] J.D. Jorgensen, B. Dabrowski, S. Pei, D.R. Richards, D.G. Hinks, Phys. Rev. B 40 (1989) 2187–2199.
[15] J. Rodríguez-Carabajal, M.T. Fernández-Díaz, J.L. Martínez, J. Phys. Condens. Matter 3 (1991) 3215–3234.
[16] S.J. Skinner, J.A. Kilner, Solid State Ionics 135 (2000) 709–712.
[17] L. Minervini, R. Grimes, J. Kilner, K. Sickafus, J. Mater. Chem. 10 (2000) 2349–2354.
[18] X. Chen, J. Yu, S.B. Adler, Chem. Mater. 17 (2005) 4537–4546.
[19] S.B. Adler, J. Am. Ceram. Soc. 84 (2001) 2117–2119.
[20] F. Prado, L. Mogni, G.J. Cuello, A. Caneiro, Solid State Ionics 178 (2007) 77–82.
[21] L. Mogni, F. Prado, G.J. Cuello, A. Caneiro, Chem. Mater. 21 (2009) 2614–2623.
[22] R. Merkle, Y.A. Mastrikov, E. Kotomin, M. Kuklja, J. Maier, J. Electrochem. Soc. 159 (2012) B219–B226.
[23] M.S.J. Islam, J. Mater. Chem. 10 (2000) 1027.
[24] L. Mogni, J. Fouletier, F. Prado, A. Caneiro, J. Solid State Chem. 178 (2005) 2715–2723.
[25] Y.A. Shilova, M.V. Patrakeev, E.B. Mitberg, I.A. Leonidov, V.L. Kozhevnikov, K.R. Poeppelmeier, J. Solid State Chem. 168 (2002) 275–283.